JBC Papers in Press. Published on April 26, 2013 as Manuscript M112.447326
The latest version is at http://www.jbc.org/cgi/doi/10.1074/jbc.M112.447326

Engineering AKAP-selective regulatory subunits of PKA through structure-based phage selection

Matthew G. Gold[1,2*], Douglas M. Fowler[3], Christopher K. Means[1], Catherine T. Pawson[1], Jason J. Stephany[3], Lorene K. Langeberg[1], Stanley Fields[3,4], John D. Scott[1,*]

[1]Howard Hughes Medical Institute, Department of Pharmacology, University of Washington School of Medicine, 1959 Pacific Ave NE, Seattle, WA 98195 USA

[2]Current address: Department of Neuroscience, Physiology & Pharmacology, University College London, Gower Street, London, WC1E 6BT UK

[3]Howard Hughes Medical Institute, Department of Genome Sciences, [4]Department of Medicine, University of Washington School of Medicine, 1959 Pacific Ave NE, Seattle, WA 98195 USA

Running Title: AKAP-selective Protein Kinase A Regulatory Subunits

*To whom correspondence should be addressed: m.gold@ucl.ac.uk, scottjdw@uw.edu

Background: Protein Kinase A (PKA) is confined to subcellular compartments by A-Kinase Anchoring Proteins (AKAPs)
Results: A structure-based phage directed evolution strategy has yielded modified type II PKA regulatory subunits with AKAP-selective binding properties
Conclusion: Engineered R_{Select} proteins preferentially target particular AKAP-PKA interfaces
Significance: R_{Select} subunits are tools to distinguish and manipulate subpopulations of anchored PKA.

SUMMARY

The cAMP-dependent protein kinase (PKA) is retained within distinct subcellular environments by the association of its type-II (RII) regulatory subunits with A-Kinase Anchoring Proteins (AKAPs). Conventional reagents that universally disrupt PKA anchoring are patterned after a conserved AKAP motif. We introduce a phage selection procedure that exploits high-resolution structural information to engineer RII mutants that are selective for a particular AKAP. Selective RII (R_{Select}) sequences were obtained for eight AKAPs following competitive selection screening. Biochemical and cell-based experiments validated the efficacy of R_{Select} proteins for AKAP2 and AKAP18. These engineered proteins represent a new class of reagents that can be used to dissect the contributions of different AKAP-targeted pools of PKA. Molecular modeling and high-throughput sequencing analyses revealed the molecular basis of AKAP-selective interactions and shed new light on native RII–AKAP interactions. We propose that this structural-directed evolution strategy might be generally applicable for the investigation of other protein interaction surfaces.

INTRODUCTION

Cellular regulation often requires that broad-spectrum enzymes are organized in a manner to optimally transduce chemical and ionic signals. Anchoring and scaffolding proteins promote such signaling efficacy by placing enzymes near substrates, and by insulating signaling units from one another (1). Most mammalian cells express 10-15 different A-Kinase Anchoring Proteins (AKAPs) that restrict the location of PKA to particular intracellular membranes or organelles (2). Similarly phosphatase targeting subunits compartmentalize protein phosphatases to spatially restrict signal termination (3). A hallmark of both classes of signal organizing proteins is the

presence of short docking sequences that associate with binding pockets on their partner enzymes (4). Structural biology and peptide array analyses have identified a consensus motif of L---A--IV--AI--A that forms the aliphatic face of an amphipathic helix on each AKAP (5,6). This region inserts into a hydrophobic groove on the surface of the docking (D/D) domain of PKA regulatory type II (RII) subunit dimer (5,6). This provides a molecular mechanism to sequester anchored pools of PKA in proximity to upstream activators (7) and in the vicinity of downstream substrates (8). As a result, this broad-spectrum kinase can simultaneously and independently operate at different locations within the same cell. Likewise, the catalytic subunit of protein phosphatase 1 associates with proteins bearing the motif RV-F (9,10) whereas protein phosphatase 2B (PP2B/calcineurin) docks to proteins bearing the P-I-X-I-T motif (11,12).

In recent years reagents have been developed for the manipulation of localized signaling processes inside cells. These include a version of the yeast Ste5 scaffolding protein with an artificial binding site that reshapes the relay of information through three-tier MAP Kinase cascades (13), and a genetically encoded photoactivatable Rac GTPase that permits the inducible control of actin-based cell movement (14). Perhaps the most established form of targeted enzyme modulation has exploited the RII–AKAP interface (5,6). The original PKA anchoring disruptor peptide Ht31 (15), derived from the anchoring helix of AKAP-Lbc, was used to demonstrate a role for PKA anchoring in a range of biological processes including phosphorylation-dependent modulation of synaptic transmission (15), hormone-mediated insulin secretion from β islets (16), and maintenance of ocular lens transparency (17). A second generation of anchoring disruptor peptides was derived from spot array screens of typically 400 peptide variants of the RII-binding sequence (5). Reagents developed by this approach are more potent than Ht31 (18), and distinguish between anchored type I (19) and type II (5) PKA regulatory subunits. However, the overriding limitation of these generic PKA anchoring disruptors is their inability to discriminate between the contributions of individual AKAPs in the control of anchored signaling events. In this article we introduce a structure-based phage selection strategy that engineers RII subunit fragments that bind selectively to individual AKAP proteins. These genetically encoded AKAP-selective probes provide tools to manipulate PKA responsive processes that are directed by individual anchoring proteins. The approach is applicable to other shared protein interaction surfaces where high-resolution structural information is available.

EXPERIMENTAL PROCEDURES

Protein purification- Purification of ~60 amino acid regions containing RII-anchoring helices was successfully attempted for ten out of sixteen different AKAPs. The sixteen AKAPs comprise AKAPs 1 through 14 as designated by the HUGO gene nomenclature committee, MAP2 and WAVE1. The fragments were synthetically amplified (20) and ligated into pGEX6P1 for bacterial expression as fusions at the C-terminus of GST (Supplementary Table S1). GST-AKAP fragments were purified by affinity to Glutathione Sepharose and gel filtration. R_{Select}AKAP18FL was expressed and purified using a similar procedure but eluting from Glutathione Sepharose by incubation with PreScission protease rather than L-glutathione. R_{Select} D/D domains (residues 1-45) were expressed with an N-terminal PreScission-cleavable 6xHis-tag and C-terminal V5 tag in pET28m and purified by nickel affinity and gel filtration. Overlays were performed with 1:10,000 w/v RII/R_{Select} subunits in TBS-T supplemented with 10 % milk. Binding was detected with 1:5,000 w/v anti-V5-HRP conjugate antibody (Invitrogen).

Mutant RII-phage library generation- RII phage were generated using the T7 select system (Novagen). PKA RIIα (1-45) with the ten-amino acid N-terminal linker SGSGSSGGSG was inserted after residue Asn351 of the T7 capsid protein by ligation into T7Select10-3b EcoR1/HindIII vector arms (Novagen). Primers were used to amplify the following DNA template prior to ligation:

GTTCTTCTGGTGGTTCTGGTATGTCTCAC**A**
TCCAG**ATC**CCGCCGGGTCTG**ACC**GAACTG

CTG**<u>CAG</u>**GGTTACACCGTTGAAGTTCTGCGT CAGCAGCCGCCGG

Bold underlined bases code for RII positions 3, 5, 10 and 14: The template oligonucletide was synthesized with a random mix (25 % of each nucleotide) at these 12 positions (Trilink Biosciences) to generate the RII-variant library. Since there are 4^{12} total DNA variants, the library coverage = $1 - (16777215/16777216)^n$, where *n* is the packaging number. 8.8 x 10^7 inserts were packaged into the phage, so ~ 99.5 % of all possible DNA variants are represented in the library. Given the redundancy of the genetic code, the coverage of total protein variants is approaching 100 %.

Phage selection- All steps were performed in Phage Wash Buffer (PWB): 25 mM Tris pH 7.2, 150 mM NaCl, 0.05 % Tween-20, 2 mM DTT, 0.5 mM EDTA. Prior to each round of selection, 0.125 µL Glutathione Magnetic beads (Pierce) were incubated with 0.1 µg of a single GST-AKAP fusion protein. After washing in 3 x 1 mL PWB, ~ 10^{10} RII-phage were input in each round of selection in the presence of 40 µg peptide aliquots corresponding to the anchoring helices of the fifteen AKAPs that were not immobilized (Supplementary Table S1). Although AKAP identification is ongoing, we reasoned that this comprehensive list of competitors would drive the selection towards the most selective RII-variant for each AKAP. Following washing in 6 x 1 mL PWB, phage were eluted by 2 h incubation with 0.5 µg PreScission protease (GE Healthcare) in 100 µL PWB. Eluates were incubated for 10 min with 2 µL Glutathione Magnetic beads to remove residual PreScission protease, then amplified to serve as the input in the next round of selection. The mutant RII sequence of phage present in eight plaques from the sixth/eighth round of selection were amplified by PCR and subjected to Sanger sequencing (Supplementary Table S2). For screens with medium selection pressure, the quantity of each free AKAP competitor peptide was reduced to 2 µg. When screening in the absence of competitors, 1 µg of GST-AKAP bound to 0.5 µL Magnetic Glutathione Phage was used as the bait.

Amplified Luminescent Proximity Homogenous Assay (AlphaScreen)- Assays were performed in 40 µL total volume with buffer consisting of 20 mM HEPES pH 7.2, 100 mM NaCl, 0.1% BSA. Dissociation constants (K_d) for AKAP – PKA D/D interactions were determined using the AlphaScreen competition-binding assay. Biotinylated R subunit D/D domains (0.3 nM, 'tracer') were incubated with fusions of GST and the RII-binding regions of AKAP2 or AKAP18 (3 nM, 'target') with increasing concentrations of untagged R subunit D/D domain. At these concentrations, the IC_{50} for disruption with untagged R D/D domain approximates the K_d of its interaction with the AKAP target. To quantify R_{Select}AKAP18 and R_{Select}AKAP2 selectivity, fusions of GST and the RII-binding regions of either AKAP2 (1 nM) or AKAP18 (1 nM) were incubated with biotinylated R_{Select} subunit D/D domains (10 nM) in the presence of increasing concentrations of AKAP competitor peptides. For GST-AKAP2, the competitor peptides consisted of an equimolar mixture of AKAP18, AKAP-Lbc, and AKAP150. For GST-AKAP18, the competitor peptides consisted of an equimolar mixture of AKAP2, AKAP-Lbc, and AKAP150. In all cases, following 1 h incubation at 4°C, streptavidin donor beads (20 ng/uL) and Anti-GST acceptor beads (20 ng/uL) (PerkinElmer) were added. Assays were incubated for 2 h prior to measurement of fluorescence at 570 nM. Analysis was performed by fitting data according to one site competition in GraphPad Prism.

Cell culture, pull-down, imaging and FRET experiments- HEK293 cells were cultured in Dulbecco's Modified Eagle Medium (DMEM) supplemented with 10 % (v/v) fetal bovine serum and penicillin/streptomycin. Cells were transfected overnight using Transit-LT1 (Mirus). Pull-down experiments were performed with 2 µg anti-FLAG or anti-V5 antibody (Sigma), supplementing with 0.4 µg R_{Select}AKAP18FL and either plus or minus 2.5 µg (10 µM) Ht31 peptide as appropriate. Associated PKA C subunits were eluted by incubation with 1 mM cAMP. Staining of FLAG-AKAP18 and AKAP2-V5 was performed by incubation with rabbit anti-V5 and mouse anti-FLAG primary antibodies, and Fluor 568 donkey anti-rabbit and Alexa Fluor 488 goat anti-mouse secondary antibodies (Invitrogen). Imaging was

performed with a Zeiss LSM 510 META confocal microscope. For FRET measurements, dual emission FRET images were obtained using a Leica DMI6000B equipped with a Dual-View image splitter (Photometrics), S470/30 and S535/30 emission filters, and 505 dcxr dichroic mirror (Chroma). Metamorph imaging software was used to quantify the FRET images using the fully specified bleed-through correction method.

Structural modeling- Models of R_{Select} – AKAP complexes were generated using the RII D/D – AKAP-*is* structure (5) as a template. The mutated protein complex structures were manually refined using the $2F_o - F_c$ electron density map of the RII D/D – AKAP-*is* crystal structure as a reference in Coot (21). Cartoon representations were generated using PyMol (DeLano Scientific).

Illumina library preparation, sequencing and quality filtration- Phage library DNA was isolated by phenol-chloroform extraction and ethanol precipitation. 50 ng of phage DNA was amplified using DF-97_PCR_long_p1F and DF-154_PCR_p1R primers (Supplementary Table S3). Libraries prepared from the fourth round of selection AKAP18 with competitors, the third round of selection without competitors and the input phage were sequenced using a HiSeq 2000 (Illumina) with DF-154_SEQ_F and DF-154_SEQ_R primers (Supplementary Table S3).

High-throughput sequencing data analysis- Sequencing data analysis was carried out using the Enrich software package (22,23). Standard Enrich output was generated using the configuration parameters detailed in **Supplementary Methods**. An average Illumina quality score was calculated for each read in a given set of paired end reads, and pairs that had an average Phred quality score of less than 20 for either read were removed. Read pairs were merged into a single sequence, and sequences failing to meet several quality criteria were discarded. Unique sequences (variants) from each library were identified and their frequency computed. Variants supported by less than ten reads were removed. Log-transformed variant enrichment ratios (E) were calculated as described[37]. Unlinked mutation scores for the i^{th} position and the j^{th} amino acid ($U_{i,j}$) were calculated as follows:

$$U_{i,j} = \sum F_{i,j}$$

These were divided by the sum of all unlinked mutation scores to the produce unlinked amino acid frequency for the i^{th} position and the j^{th} amino acid ($Fu_{i,j}$):

$$Fu_{i,j} = \frac{U_{i,j}}{\sum U}$$

The unlinked enrichment ratio for the i^{th} position and the j^{th} amino acid between the input library and the X^{th} round ($E_{unlinked,i,j,X}$) was calculated as follows:

$$E_{unlinked,i,j,X} = \frac{Fu_{i,j,X}}{Fu_{i,j,input}}$$

The selectivity index was calculated for the i^{th} position and the j^{th} amino acid between the AKAP18 library in the presence or absence of AKAP competitor peptide ($SI_{i,j}$) as follows:

$$SI_{i,j} = E_{unlinked,i,j,+competitor} - E_{unlinked,i,j,-competitor}$$

Extended experimental procedures are included in **Supplementary Methods.**

RESULTS

Rational structure-based construction of a RII-variant phage library- AKAPs contain a 16-residue sequence that is necessary and sufficient for PKA anchoring (18,24). Conserved aliphatic side-chains within this sequence provide the hydrophobic face of an amphipathic helix. These residues participate in Van der Waals interactions with a reciprocal binding groove formed by the docking domains of the RII dimer (5,6) (Fig. 1*A*). Competitor peptides that mimic the AKAP side of this protein-protein interface universally uncouple PKA anchoring irrespective of which AKAP is involved (18). High-resolution crystal structures of RII-AKAP peptide complexes indicate that non-conserved side-chains in the AKAP helix bond with Ile3, Ile5, Thr10 and Gln14 of each RIIα protomer (Fig. 1*B*). We reasoned that systematically engineering these positions might

introduce AKAP-selective binding determinants into RII.

On the basis of this postulate, we devised a phage display selection for AKAP-specific RII variants. An RIIα (1-45) fragment encompassing the D/D domain was fused to the C-terminus of the T7 bacteriophage capsid protein via a ten-amino acid linker (Supplementary Fig. S1*A*). In pilot studies GST–AKAP79 recovered 300-fold more RII-phage that GST alone (Supplementary Fig. S1*B*). In a more stringent test, successive rounds of binding to an immobilized AKAP79 fragment followed by phage amplification selected native RII-phage from a starting pool that contained a 1000-fold molar excess of an anchoring-defective (T17W) RII form (Supplementary Fig. S1*C*-S1*F*). Taken together, these experiments attest to the feasibility of this approach.

Next RII D/D inserts were amplified from a DNA template with random nucleotides encoding positions 3, 5, 10 and 14. RII mutant sequences were packaged into phage to construct a T7 capsid-display library with greater than 99% of the 160,000 (4^{20}) possible RII mutant sequences (25). High-throughput sequencing confirmed that every amino acid was represented at positions 3, 5, 10 and 14 in RII (Fig. 1*C*, red) and that the wild-type amino acids persisted in the remainder of the fragment (Fig. 1*C*, blue). Further inspection of the high-throughput sequencing data confirmed that nucleotide variation was limited to the codons of interest (Fig. 1*D*); that the majority of RII-phage encoded mutations at four positions compared to wild-type (Fig. 1*E*); and that there was comprehensive coverage of all the possible RII mutant sequences (Fig. 1*F*).

Competitive screening for AKAP-selective RII mutants- Isolation of phage expressing AKAP-selective RII variants involved competitive screening using a panel of purified AKAP fragments (Fig. 2*A* & Supplementary Table S1). This procedure was conducted in four steps. First, glutathione magnetic beads were charged with the GST-AKAP fragment of interest. This immobilized bait was incubated with the phage library in the presence of free competitor anchoring helices from the fifteen AKAPs (step 1, Fig. 2*B*). A wash phase in step 2 removed free and AKAP-competitor-associated phage (step 2, Fig. 2*B*). PreScission protease cleavage in step 3 liberated AKAP-RII phage complexes from the glutathione beads (step 3, Fig. 2*B*). Recovered phage were amplified in step 4 to serve as the input for the next round of selection. This stepwise cycle was repeated 6-8 times until the selected material converged into a single RII sequence as determined by Sanger sequencing (Supplementary Table S2).

This screening process was performed with ten different GST-AKAP fragments as bait. Predominant RII-variant sequences emerged for AKAP2, AKAP150, AKAP18, AKAP-Lbc and AKAP220 when screens were performed under high selection pressure (5,000-fold molar excess of each competitor AKAP, Fig. 2*C*, *top section*). Phage recovery was at background levels for the remaining five AKAPs. However mutant RII sequences for mAKAP, Gravin and MAP2 were forthcoming when screens were performed with a less stringent selection protocol (250-fold molar excess of each competitor AKAP, Fig. 2*C*, *middle section*). Isolation of RII variants for the low affinity anchoring proteins AKAP95 and WAVE-1 were successful in the absence of AKAP competitor peptides (Fig. 2*C*). Collectively, our screening process yielded 10 unique variant RII sequences selective for individual AKAPs (Fig. 2*C*, *right column*). Each modified sequence contains substitutions at positions 3, 5, 10 or 14 of RII (Fig. 2*C*, *right column*).

R_{Select} subunits exhibit AKAP selectivity- Biochemical validation of AKAP-selectivity was limited to engineered RII 1-45 variants with a preference for AKAP2, AKAP150 and AKAP18. These proteins were designated **RII** AKAP-**Select**ive (R_{Select}) subunits. Each C-terminal V5 tagged R_{Select} D/D domain was expressed in bacteria and purified by nickel affinity and gel filtration chromatography (Fig. 3*A*). The fidelity of these R_{Select} D/D domain fragments was tested by far-western blotting against a collection of the PKA anchoring domains from ten different AKAPs (Fig. 3*B*, *top panel*). R_{Select}AKAP2 and R_{Select}AKAP18 preferentially bound to their cognate AKAP binding partners (Fig. 3*B*, *second & third panels*). In contrast, R_{Select}AKAP150 exhibited an intermediate selectivity with a binding preference for AKAP150, AKAP18 and AKAP220 (Fig. 3*B*, *fourth panel*). Control

experiments confirmed that wild-type RII 1-45 bound each AKAP fragment in the overlay assay (Fig. 3*B*, *bottom panel*).

We further investigated the binding affinities of R_{Select}AKAP2 and R_{Select}AKAP18 using AlphaScreen (Amplified Luminescent Proximity Homogenous Assay). Dissociation constants were measured for AKAP18 using either RII or R_{Select}AKAP18 as the ligand. Wild-type RII bound AKAP18 with a K_d of 16.3 ± 1.1 nM (n=3), whereas R_{Select}AKAP18 exhibited a lower affinity for the anchoring protein (K_d 161.9 ± 23.3 nM, n=3, $p<0.05$, Fig. 3*C*). However, when in the presence of a mixture of competitor AKAP peptides, the AKAP18-R_{Select}AKAP18 complex was 4.4-fold more resistant to disruption than the wild-type complex (Figs. 3*D & E,* n=3, p=0.043). Thus, although R_{Select}AKAP18 binds its anchoring protein with reduced affinity, this engineered form has greater selectivity for AKAP18 than wild-type RII.

We took advantage of this latter property to further test the efficacy of R_{Select}AKAP18 binding to its preferred anchoring protein. We reasoned that PKA holoenzymes formed with R_{Select}AKAP18 should remain attached to the anchoring protein, even in the presence of the PKA anchoring disruptor peptide Ht31 (24). Mutations were introduced at positions 3, 5, 10 and 14 of the full-length regulatory subunit to generate R_{Select}AKAP18FL (Fig. 3*F*). This modified PKA holoenzyme remained anchored to AKAP18 in the presence of Ht31 (Fig. 3*G*). Western blotting detected C subunit in AKAP18 immune complexes (Fig. 3*G, top panel, lane 7*). Control experiments confirmed that R_{Select}AKAP18FL did not enhance the co-fractionation of the C subunit with AKAP2 under the same conditions (Fig. 3*G*, lanes 2-4). Likewise, AlphaScreen measurements revealed reduced binding affinity but enhanced selectivity of R_{Select}AKAP2 for its preferred anchoring protein when compared to wild-type RII (Fig. 3*H-J*). Wild-type RII subunits (K_d = 12.5 ± 1.8 nM, blue in Fig. 3*H*) bind AKAP2 with significantly ($p < 0.05$) higher affinity that R_{Select}AKAP2 (K_d = 246.6 ± 18.6 nM, red in Fig. 3*H*). However, whereas a competitor AKAP peptide mixture disrupted the interaction between AKAP2 and wild-type RII with an IC_{50} = 0.68 ± 0.05 μM (blue in Fig. 3*I* & 3*J*), the AKAP2-R_{Select}AKAP2 complex was significantly more resistant to disruption by 3.4-fold (n=3; $p<0.05$) according to IC_{50} (2.3 ± 0.16 μM, red in Fig. 3*I* & 3*J*).

Most AKAPs contain targeting motifs that associate with structural proteins or cellular membranes (26). We exploited this property to validate the cellular efficacy of R_{Select}AKAP2 and R_{Select}AKAP18 (Fig. 4). Immunofluorescence staining of fixed HEK293 cells showed AKAP2 enriched in perinuclear and reticular regions (17) whereas AKAP18δ is concentrated in the nucleus (27) (Figs. 4*A* & 4*B*). The segregation of these AKAP signals can be seen in the composite image (Fig. 4*C*). These staining patterns were recapitulated in cells co-transfected with genetically encoded fluorescent R_{Select} D/D fragments (Figs. 4*D*-4*F*): R_{Select}AKAP2-Cherry adopted a reticular staining pattern (Fig. 4*E*) whereas R_{Select}AKAP18-YFP was predominantly nuclear (Fig. 4*D*). The nuclear localization of R_{Select}AKAP18 D/D was retained in the presence of wild-type RII-RFP (Figs. 4*G*-4*I*). The important conclusion that can be drawn from these studies is that these R_{Select} fragments have identical subcellular distributions to their AKAP binding partners, implying that they can find their cognate AKAPs in situ.

To further test the selectivity of R_{Select}AKAP18 we employed fluorescence resonance energy transfer (FRET) to evaluate its binding to AKAP18δ or the PKA anchoring protein MAP2 (28). This approach allows detection of protein proximity below the diffraction limit of light in living cells (29). As expected, both AKAP18δ-CFP and MAP2-CFP were capable of eliciting a FRET signal when paired with wild-type RII-YFP (Figs. 4*J*, 4*K*, and 4*N* lanes 1 & 2). However, only AKAP18δ-CFP was capable of FRET when paired with R_{Select}AKAP18-YFP (Figs. 4*L*, 4*M* and 4*N* lanes 3 & 4). Comparison of R_{Select}AKAP18-FRET / RII-FRET ratios confirmed that R_{Select}AKAP18 preferentially recognizes AKAP18δ (0.57 ± 0.22) over MAP2 (0.03 ± 0.02) (Fig. 4*O*). Taken together, the far-western blotting, fixed- and live-cell imaging data validate the selectivity of these R_{Select} molecules.

A molecular basis for high affinity RII interaction with AKAP18- Systematic amino acid substitution

at all positions of 16 residue AKAP helices has been invaluable in identifying determinants for R subunit interaction by immobilized peptide array (5,18,30). This experimental strategy was not feasible for analysis of the reciprocal binding surface since correct folding of the RII D/D is necessary to create the four helix AKAP-binding groove. Therefore, high-throughput DNA sequencing of RII-variant libraries before and after selection using AKAP18 (23) was utilized for a comprehensive structure-function analysis of the RII binding surface (Fig. 5*A*, blue). We reasoned that phage selection with AKAP18 alone could reveal which amino acids on RII favor high-affinity interaction with this anchoring protein. After three rounds of selection using AKAP18 as bait, sequence-function maps were compiled (Fig 5*A*). This analysis indicated the change of frequency of amino acids at positions 3, 5, 10 and 14 of RII upon successive rounds of selection. Although the wild-type residue, Ile was present at position 3, other side chains were also tolerated. The branched aliphatic amino acids Ile and Val were enriched at position 5. These data confirm that positions 3 and 5 on RII contribute to the integrity of the hydrophobic binding surface of the docking and dimerization domain (5,6,30). In contrast, side-chains with the capacity to hydrogen bond emerged at positions 10 and 14 (Fig. 5*A*, blue). Hence we conclude that these hydrophilic interactions enhance the recruitment of AKAP18 (Fig. 5*B*).

A molecular basis for R_{Select}-binding preference

Three-dimensional structures of RII–AKAP complexes (5,6) provide a molecular framework for understanding the binding preferences of R_{Select} proteins. The likely contact points between residues 3, 5, 10 & 14 of RII and the reciprocal side-chains on an AKAP helix (high variability positions) are shown in Figure 6*A*. A structural model of this protein-protein interface was assembled by substitution and refinement of the 1.3 Å RII dimer–AKAP-*is* crystal structure (5) (Figs. 6*B* & 6*C*). One striking feature is that lysines 10 and 19, which project from alternate sides of the AKAP18 amphipathic helix, are optimally aligned to form salt-bridge interactions with Asp10 in each R_{Select}AKAP18 protomer (Figs. 6*B* & 6*C*). Scrutiny of the aligned RII-binding sequences from ten AKAPs (Fig. 6*A*) reveals that only AKAP18 incorporates lysines on both sides of its anchoring helix. This could explain why aspartate was selected at position 10 in R_{Select}AKAP18. Interestingly, AKAP18 is unique in orienting additional leucines at positions 8 and 18 in its anchoring helix (Fig. 6*A*). Our structural model suggests that these aliphatic side chains interact with Val3 and Leu5 in R_{Select}AKAP18 (Figs. 6*B* & 6*C*). Molecular models were also compiled for R_{Select}AKAP2 and R_{Select}AKAP150 complexes (Supplementary Fig. S2). Each simulation predicts that increased complementarity between variable R_{Select} positions and cognate AKAP side-chains is an important component of discrimination that is introduced into these engineered RII subunits. For example, Arg10 and Arg14 on each R_{Select}AKAP2 protomer are positioned to hydrogen bond with Gln14, Asn15, Gln18 and Gln19 in AKAP2 (Supplementary Figs. S2*A*-S2*C*). Likewise, Gln10 in R_{Select}AKAP150 can form a hydrogen-bonding network with Ser10 and Lys14 in AKAP150 (Supplementary Figs. S2*A*, S2*D* & S2*E*). This latter model also predicts that Arg5 of R_{Select}AKAP150 forms a salt-bridge with Glu18 in AKAP150 (Supplementary Figs. S2*A*, S2*D* & S2*E*).

To consolidate predictions from the AKAP18–R_{Select}AKAP18 structural model in an empirical manner we performed further sequence-function analysis in the presence of AKAP competitor peptides. The enrichment ratios for each amino acid at positions 3, 5, 10 and 14 in RII, in an early round of selection in the presence of competitors are shown in Figure 5 (red triangles). Inclusion of peptide competitors increased the stringency of selection. This enhanced the selection of leucine at position 5, aspartate at position 10 and glutamate at position 14 of RII (Fig. 6*D* & 6*E*). Selectivity plots were calculated by dividing AKAP18 enrichment-ratios in the presence of competitors by the enrichment-ratios without competitors (Figs. 6*F*-6*I*). These plots show that Leu5 and Asp10 are the most AKAP18-discerning side chains (Figs. 6*G* & 6*H*). Conversely, these residues are not strongly selected in the absence of competitors (Figs. 5 blue & 6*D*). This implies that the inclusion of Leu5 and Asp10 has a negative effect on R_{Select}AKAP18 binding to other AKAP family members. This conclusion is consistent with the results of the R subunits overlays (Fig. 3*B*) and K_d

measurements (Figs. 3*E* & 3*F*), which show that R_{Select}AKAP18 binds to AKAP18 with lower affinity than wild-type RII in the absence of other AKAPs. Although aspartate is the most AKAP18-selective residue at position 14 in this analysis (Fig. 6*I*), the predominant R_{Select}AKAP18 sequence that emerged after eight rounds of selection contained glycine at position 14. This suggests that one, but not two, negative charges on alternate sides of the AKAP18 anchoring helix provide optimal selectivity, and that Gly14 may cooperate with Asp10 to enable formation of salt bridges between the acidic residue and lysines on either side of the AKAP18 anchoring helix (Figs. 6*B* & 6*C*). In sum, the modeling and high-throughput sequencing analysis support our initial hypothesis that mutations in RII positions 3, 5, 10 and 14 can impart AKAP-selective properties.

DISCUSSION

On the basis of high-resolution structures of the AKAP-PKA interface, we generated a phage library bearing 160,000 variants of the RII D/D domain. Following the protocol outlined in Figure 2*B*, we enriched for RII variants with selectivity for a particular AKAP. The efficacy of this approach is demonstrated in Figures 3 & 4 by the preferential association of R_{Select} subunits with their cognate AKAPs *in vitro* and *in vivo*. High-throughput sequencing analysis when combined with structural modeling has provided a clearer understanding of which side chains on RII enhance association with individual AKAPs. Comparative analysis of AKAP18 selections in the presence and absence of competitors showed that residues in the optimal R_{Select} sequence are both compatible with residues in the high-variability positions of the target AKAP and incompatible with the equivalent positions in off-target AKAPs.

In addition, sequence-function analysis presented in figure 5 revealed that hydrophilic contacts facilitated by positions 10 and 14 in RII are more critical for interaction with AKAP18 than positions 3 and 5. Inspection of crystal structures of the RII-AKAP-*is* and the RII-D-AKAP2 complexes (5,6) reveals that Thr10 on a single RII protomer forms a water-mediated hydrogen bond with the backbone carbonyl of Ile12 in the AKAP-helix. Thr at position 10 favors high-affinity interaction with AKAP18 in comparison to the sterically similar side chains Val and Ile (Fig. 5). Therefore this hydrophilic contact is likely to be an important component of all RII-AKAP interfaces. The influence of this hydrophilic quadrad that comprises the core of the D/D domain should be factored into attempts to generate small molecules that disrupt AKAP-RII interactions (31).

Our intermolecular FRET measurements indicate that R_{Select} subunits are viable chemical biology reagents that selectively associate with AKAPs in living cells. R_{Select}AKAP18-YFP and AKAP18δ-CFP must be within ~80 Å to permit fluorescence resonance energy transfer (29) (Figs. 4*J*-4*O*). Since C-terminal epitope tagging does not impair the ability of R_{Select}AKAP18 to recognize its anchoring protein inside cells, chemical or biological reporters may be fused to R_{Select} subunits. Fusion of chemical moieties such as photoactivatable-GFP or phosphorylation-sensitive FRET reporters (32) may ultimately permit the monitoring of movement and the activity of subpopulations of PKA associated with a given AKAP. Similarly, fusion of biologically active molecules such as PKA catalytic subunit or cAMP phosphodiesterase to a given R_{Select} subunit may enable controlled up or down-regulation of PKA activity within the immediate vicinity of a particular AKAP complex. Prospective delivery methods include transfection, genomic incorporation (33), and inclusion of purified R_{Select} D/D in the patch pipette in a manner analogous to generic PKA anchoring disruptor reagents (5). Since wild-type RII binds to AKAP2 and AKAP18 with significantly higher affinity than the respective R_{Select} subunits for these AKAPs, the best approach may be to apply the R_{Select} subunits in tandem with Ht31 (Fig. 3*H*) to determine whether individual AKAPs are sufficient for targeting PKA to particular ion channels. Future biological questions to address using R_{Select}-based reagents include establishing the relative contributions of individual AKAP-anchored subpopulations of PKA that regulate synaptic transmission (34,35) and control cardiac excitation-contraction coupling (36). AKAP-selective PKA disruptors have also been conjectured as forerunners of the next generation of drugs that target the β-adrenergic system in the heart (37). Hence the continued development of R_{Select} reagents may contribute to target validation of these new therapeutic agents.

In a broader context, we anticipate that our structure-based phage selection procedure may enable development of synthetic biology reagents for studying other functionally important signaling protein interactions. The most promising candidate interfaces are those for which high-resolution structural information is available to guide the design of mutant libraries. Theoretically the T7Select system could also accommodate more complex phage libraries containing at least five randomized positions (20^5 =3.2 x 10^6 combinations) within the target sequence. Display of molecules larger than 45 amino acids is also possible using T7 bacteriophage. Thus, it may be possible to design mutant libraries for intact proteins such as phosphatase catalytic subunits that selectively recognize PP1 targeting subunits by virtue of the RV-F motif (38) or calcineurin/PP2B anchoring proteins that work through P-I-X-I-T motifs (11,12). The development of such reagents will facilitate spatial manipulation of enzyme activities and aid in our understanding of normal and pathological signaling processes.

Acknowledgements- This work was supported by the National Institutes of Health (grant P41GM103533 to SF, F32GM084699 to DMF, and GM48231 to JDS), and a Sir Henry Wellcome Postdoctoral Research Fellowship to MGG. CKM is supported by National Institutes of Health Experimental Pathology of Cardiovascular Disease training grant T32 HL 07312.

REFERENCES

1. Pawson, C. T., and Scott, J. D. (2010) Signal integration through blending, bolstering and bifurcating of intracellular information. *Nat Struct Mol Biol* **17**, 653-658
2. Welch, E. J., Jones, B. W., and Scott, J. D. (2010) Networking with AKAPs: context-dependent regulation of anchored enzymes. *Mol Interv* **10**, 86-97
3. Roy, J., and Cyert, M. S. (2009) Cracking the phosphatase code: docking interactions determine substrate specificity. *Sci Signal* **2**, re9
4. Gold, M. G., Barford, D., and Komander, D. (2006) Lining the pockets of kinases and phosphatases. *Curr Opin Struct Biol* **16**, 693-701
5. Gold, M. G., Lygren, B., Dokurno, P., Hoshi, N., McConnachie, G., Tasken, K., Carlson, C. R., Scott, J. D., and Barford, D. (2006) Molecular basis of AKAP specificity for PKA regulatory subunits. *Mol Cell* **24**, 383-395
6. Kinderman, F. S., Kim, C., von Daake, S., Ma, Y., Pham, B. Q., Spraggon, G., Xuong, N. H., Jennings, P. A., and Taylor, S. S. (2006) A dynamic mechanism for AKAP binding to RII isoforms of cAMP-dependent protein kinase. *Mol Cell* **24**, 397-408
7. Bauman, A. L., Soughayer, J., Nguyen, B. T., Willoughby, D., Carnegie, G. K., Wong, W., Hoshi, N., Langeberg, L. K., Cooper, D. M., Dessauer, C. W., and Scott, J. D. (2006) Dynamic regulation of cAMP synthesis through anchored PKA-adenylyl cyclase V/VI complexes. *Mol Cell* **23**, 925-931
8. Keely, S. L. (1977) Activation of cAMP-dependent protein kinase without a corresponding increase in phosphorylase activity. *Res Commun Chem Pathol Pharmacol* **18**, 283-290
9. Egloff, M. P., Johnson, D. F., Moorhead, G., Cohen, P. T., Cohen, P., and Barford, D. (1997) Structural basis for the recognition of regulatory subunits by the catalytic subunit of protein phosphatase 1. *EMBO J* **16**, 1876-1887
10. Terrak, M., Kerff, F., Langsetmo, K., Tao, T., and Dominguez, R. (2004) Structural basis of protein phosphatase 1 regulation. *Nature* **429**, 780-784
11. Gold, M. G., Stengel, F., Nygren, P. J., Weisbrod, C. R., Bruce, J. E., Robinson, C. V., Barford, D., and Scott, J. D. (2011) Architecture and dynamics of an A-kinase anchoring protein 79 (AKAP79) signaling complex. *Proc Natl Acad Sci U S A* **108**, 6426-6431
12. Li, H., Pink, M. D., Murphy, J. G., Stein, A., Dell'acqua, M. L., and Hogan, P. G. (2012) Balanced interactions of calcineurin with AKAP79 regulate Ca(2+)-calcineurin-NFAT signaling. *Nat Struct Mol Biol*
13. Bashor, C. J., Helman, N. C., Yan, S., and Lim, W. A. (2008) Using engineered scaffold interactions to reshape MAP kinase pathway signaling dynamics. *Science* **319**, 1539-1543
14. Wu, Y. I., Frey, D., Lungu, O. I., Jaehrig, A., Schlichting, I., Kuhlman, B., and Hahn, K. M. (2009) A genetically encoded photoactivatable Rac controls the motility of living cells. *Nature* **461**, 104-108
15. Rosenmund, C., Carr, D. W., Bergeson, S. E., Nilaver, G., Scott, J. D., and Westbrook, G. L. (1994) Anchoring of protein kinase A is required for modulation of AMPA/kainate receptors on hippocampal neurons. *Nature* **368**, 853-856
16. Lester, L. B., Langeberg, L. K., and Scott, J. D. (1997) Anchoring of protein kinase A facilitates hormone-mediated insulin secretion. *Proc Natl Acad Sci U S A* **94**, 14942-14947
17. Gold, M. G., Reichow, S. L., O'Neill, S. E., Weisbrod, C. R., Langeberg, L. K., Bruce, J. E., Gonen, T., and Scott, J. D. (2012) AKAP2 anchors PKA with aquaporin-0 to support ocular lens transparency. *EMBO Mol Med* **4**, 15-26
18. Alto, N. M., Soderling, S. H., Hoshi, N., Langeberg, L. K., Fayos, R., Jennings, P. A., and Scott, J. D. (2003) Bioinformatic design of A-kinase anchoring protein-in silico: a potent and selective peptide antagonist of type II protein kinase A anchoring. *Proc Natl Acad Sci U S A* **100**, 4445-4450

19. Carlson, C. R., Lygren, B., Berge, T., Hoshi, N., Wong, W., Tasken, K., and Scott, J. D. (2006) Delineation of type I protein kinase A-selective signaling events using an RI anchoring disruptor. *J Biol Chem* **281**, 21535-21545
20. Grote, A., Hiller, K., Scheer, M., Munch, R., Nortemann, B., Hempel, D. C., and Jahn, D. (2005) JCat: a novel tool to adapt codon usage of a target gene to its potential expression host. *Nucleic Acids Res* **33**, W526-531
21. Emsley, P., Lohkamp, B., Scott, W. G., and Cowtan, K. (2010) Features and development of Coot. *Acta Crystallogr D Biol Crystallogr* **66**, 486-501
22. Fowler, D. M., Araya, C. L., Gerard, W., and Fields, S. (2011) Enrich: software for analysis of protein function by enrichment and depletion of variants. *Bioinformatics* **27**, 3430-3431
23. Fowler, D. M., Araya, C. L., Fleishman, S. J., Kellogg, E. H., Stephany, J. J., Baker, D., and Fields, S. (2010) High-resolution mapping of protein sequence-function relationships. *Nat Methods* **7**, 741-746
24. Carr, D. W., Stofko-Hahn, R. E., Fraser, I. D., Bishop, S. M., Acott, T. S., Brennan, R. G., and Scott, J. D. (1991) Interaction of the regulatory subunit (RII) of cAMP-dependent protein kinase with RII-anchoring proteins occurs through an amphipathic helix binding motif. *J Biol Chem* **266**, 14188-14192
25. Knight, R., and Yarus, M. (2003) Analyzing partially randomized nucleic acid pools: straight dope on doping. *Nucleic Acids Res* **31**, e30
26. Scott, J. D., and Pawson, T. (2009) Cell signaling in space and time: where proteins come together and when they're apart. *Science* **326**, 1220-1224
27. Brown, R. L., August, S. L., Williams, C. J., and Moss, S. B. (2003) AKAP7gamma is a nuclear RI-binding AKAP. *Biochem Biophys Res Commun* **306**, 394-401
28. Theurkauf, W. E., and Vallee, R. B. (1982) Molecular characterization of the cAMP-dependent protein kinase bound to microtubule-associated protein 2. *J Biol Chem* **257**, 3284-3290
29. Giepmans, B. N. G., Adams, S. R., Ellisman, M. H., and Tsien, R. Y. (2006) The fluorescent toolbox for assessing protein location and function. *Science (New York, N Y)* **312**, 217-224
30. Burns-Hamuro, L. L., Ma, Y., Kammerer, S., Reineke, U., Self, C., Cook, C., Olson, G. L., Cantor, C. R., Braun, A., and Taylor, S. S. (2003) Designing isoform-specific peptide disruptors of protein kinase A localization. *Proceedings of the National Academy of Sciences of the United States of America* **100**, 4072-4077
31. Christian, F., Szaszak, M., Friedl, S., Drewianka, S., Lorenz, D., Goncalves, A., Furkert, J., Vargas, C., Schmieder, P., Gotz, F., Zuhlke, K., Moutty, M., Gottert, H., Joshi, M., Reif, B., Haase, H., Morano, I., Grossmann, S., Klukovits, A., Verli, J., Gaspar, R., Noack, C., Bergmann, M., Kass, R., Hampel, K., Kashin, D., Genieser, H. G., Herberg, F. W., Willoughby, D., Cooper, D. M., Baillie, G. S., Houslay, M. D., von Kries, J. P., Zimmermann, B., Rosenthal, W., and Klussmann, E. (2011) Small molecule AKAP-protein kinase A (PKA) interaction disruptors that activate PKA interfere with compartmentalized cAMP signaling in cardiac myocytes. *The Journal of biological chemistry* **286**, 9079-9096
32. Dodge-Kafka, K. L., Soughayer, J., Pare, G. C., Carlisle Michel, J. J., Langeberg, L. K., Kapiloff, M. S., and Scott, J. D. (2005) The protein kinase A anchoring protein mAKAP coordinates two integrated cAMP effector pathways. *Nature* **437**, 574-578
33. Harvey, C. D., Ehrhardt, A. G., Cellurale, C., Zhong, H., Yasuda, R., Davis, R. J., and Svoboda, K. (2008) A genetically encoded fluorescent sensor of ERK activity. *Proc Natl Acad Sci U S A* **105**, 19264-19269
34. Tunquist, B. J., Hoshi, N., Guire, E. S., Zhang, F., Mullendorff, K., Langeberg, L. K., Raber, J., and Scott, J. D. (2008) Loss of AKAP150 perturbs distinct neuronal processes in mice. *Proc Natl Acad Sci U S A* **105**, 12557-12562
35. Zhong, H., Sia, G. M., Sato, T. R., Gray, N. W., Mao, T., Khuchua, Z., Huganir, R. L., and Svoboda, K. (2009) Subcellular dynamics of type II PKA in neurons. *Neuron* **62**, 363-374

36. Lygren, B., Carlson, C. R., Santamaria, K., Lissandron, V., McSorley, T., Litzenberg, J., Lorenz, D., Wiesner, B., Rosenthal, W., Zaccolo, M., Tasken, K., and Klussmann, E. (2007) AKAP complex regulates Ca2+ re-uptake into heart sarcoplasmic reticulum. *EMBO Rep* **8**, 1061-1067
37. Wells, J. A., and McClendon, C. L. (2007) Reaching for high-hanging fruit in drug discovery at protein-protein interfaces. *Nature* **450**, 1001-1009
38. Bollen, M., Peti, W., Ragusa, M. J., and Beullens, M. (2010) The extended PP1 toolkit: designed to create specificity. *Trends Biochem Sci* **35**, 450-458

FIGURE LEGENDS

FIGURE 1. Construction of RII-variant phage library (A) Cartoon structural representation of low variability aliphatic residues on one face of the AKAP anchoring helix (orange) and the reciprocal binding surface in the RII D/D domain (residues 1-45, grey). (B) Residues in PKA RII that contact AKAP positions of higher variability (orange spheres). (C) Frequencies of each amino acid at every position in the first twenty amino acids of RII expressed on the surface of the phage in the input library. (D) Distribution of mutant nucleotides within the RII coding sequences of the input RII-phage library. Mutations from wild-type RII coding sequence was restricted to codons 3, 5, 10 and 14 (E) Distribution of single, double, triple and quadruple RII mutants in the input phage library (F) High-throughput sequencing statistics of RII-variant phage libraries.

FIGURE 2. Screening of AKAP-selective RII variants by phage selection (A) Coomassie-stained SDS-PAGE of GST-AKAP anchoring-helix fragments (B) Four-step iterative scheme for enrichment of RII-variant phage that are selective for a single AKAP. (C) Predominant RII-variant sequences following phage selection with each of the ten different AKAP baits. High selection pressure was 5,000-fold molar excess of each competitor AKAP helix, Medium was 250-fold molar excess of the competitors and None was in the absence of competitor fragments.

FIGURE 3. R_{Select} subunits exhibit AKAP selectivity *in vitro* (A) Coomassie-stained SDS-PAGE of purified R_{Select} 1-45 fragments (B) RII-overlay of a panel of ten GST-AKAP fusion proteins (Ponceau-stained, top row) using D/D fragments shown in (A). R_{Select}AKAP2 1-45 (second row), R_{Select}AKAP18 1-45 (third row), R_{Select}AKAP150 1-45 (fourth row) or wild-type RII 1-45 (bottom row). (C) AlphaScreen competition binding assay for AKAP18 with D/D fragments of either R_{Select}AKAP18 (red) or RII WT (blue) and increasing concentrations of the appropriate untagged R subunit. K_d (n=3) of AKAP18 interaction with either R_{Select}AKAP18 (red) or RII WT (blue) is shown. (D) Competition binding assay for AKAP18 with D/D fragments of either R_{Select}AKAP18 (red) or RII WT (blue) in the presence of increasing concentrations of a competitor AKAP peptide mixture. (E) The IC_{50} (n=3) concentration of the competitor AKAP peptide mixture for AKAP18 associated with either R_{Select}AKAP18 (red) or RII WT (blue). (F) Coomassie-stained SDS-PAGE of the purified full length mutant RII: R_{Select}AKAP18FL. (G) Immunoprecipitations from HEK293 cell lysates were performed in the presence (lanes 4 & 7) or absence (lanes 1-3, 5-6) of R_{Select}AKAP18FL using either IgG (lane 1), anti-V5 antibody (lanes 2-4, for V5-AKAP2) or anti-FLAG antibody (lanes 5-7, for FLAG-AKAP18δ). These were done either with Ht31 (lanes 3, 4, 6 & 7) or without Ht31 (lanes 1, 2, & 5). Anchoring and co-precipitation of the modified PKA holoenzyme was tested by immunoblotting for the PKA C subunit. Immunoprecipitation of AKAP18δ (anti-FLAG), AKAP2 (anti-V5) and PKA C was confirmed by immunoblotting (middle and bottom blots). (H) AlphaScreen competition binding assay for AKAP2 with either R_{Select}AKAP2 (red) or RII WT (wild-type, blue) and increasing concentrations of the appropriate untagged R subunit. The K_d (n=3) of AKAP2 interaction with either R_{Select}AKAP2 or RII WT is indicted. (I) AlphaScreen competition binding assay for AKAP2 with either R_{Select}AKAP2 (red) or RII WT (blue) in the presence of increasing concentrations of a competitor AKAP peptide mixture. (J) The IC_{50} (n=3) concentration of the competitor AKAP peptide mixture for AKAP2 associated with either R_{Select}AKAP2 (red) or RII WT (blue).

FIGURE 4. R_{Select} subunits exhibit AKAP selectivity in cells (A-I) Confocal images of full length AKAPs and R_{Select} D/D fragments show their subcellular location. Immunofluorescent images of HEK293 cells co-transfected with FLAG-AKAP18δ (A, green in C) and AKAP2-V5 (B, red in C). Fluorescent images show R_{Select}AKAP18-YFP (D, yellow in F) and R_{Select}AKAP2-Cherry (E, red in F), which were co-expressed with AKAP18δ and AKAP2. Fluorescent images of R_{Select}AKAP18-YFP (G, yellow in I) and RII-RFP (H, red in I), which were co-expressed with AKAP18δ. (J – M) CFP-YFP FRET imaging of the following AKAP – RII or R_{Select}AKAP18 pairs in HEK293 cells: AKAP18δ-CFP and RII-YFP (J);

MAP2-CFP and RII-YFP (K); AKAP18δ-CFP and R_{Select}AKAP18-YFP (L); and MAP2-CFP and R_{Select}AKAP18-YFP (M). Images were acquired for donor CFP (left column) and acceptor YFP (center column), and corrected FRET images are presented in the right column. (N) Ratiometric quantification of intermolecular FRET pairs as described in N-Q. (O) Quantification of FRET signals in AKAP18δ-CFP/R_{select}AKAP18-YFP and MAP2-CFP/R_{select}AKAP18-YFP pairs normalized to AKAP18δ-CFP/RII-YFP and MAP2-CFP/RII-YFP respectively.

FIGURE 5. Sequence-function plot of RII-variant selection with AKAP18. (A) Relative changes in frequency of each amino acid at the four variable RII positions are shown after three rounds of selection using GST-AKAP18 in either the presence (red triangles) or absence (blue circles) of competitor AKAP peptides. Amino acid mutations that increased in frequency relative to the input library have positive log transformed enrichment ratios as a consequence of improved binding. (B) Cartoon structural representation of positions 3, 5, 10 and 14 in wild-type RII in relation to an AKAP anchoring helix (orange).

FIGURE 6. Structural basis of R_{Select} selectivity (A) Alignment of AKAP anchoring helices. Variable positions are in light grey, highly conserved small aliphatic residues are in dark grey (top). RII protomer residues 3, 5, 10, and 14 are shown below with dashed lines indicating interaction with variable AKAP positions. (B & C) Cartoon representation of a structural model of R_{Select}AKAP18 in complex with the anchoring helix of AKAP18 (D & E). Logoplots of an early round of selection with AKAP18 in the absence (D) or presence (E) of competitor AKAP peptides. Amino acid mutations that increased in frequency after selection were used to generate a logo plot where the height of each amino acid indicates its frequency at that position (WebLogo, http://weblogo.berkeley.edu/). The selectivity index for each amino acid substitution is shown at positions 3 (F), 5 (G), 10 (H) and 14 (I) in the RII sequence. Black circles indicate selectivity index scores; blue squares denote wild-type RII amino acids; and red squares denote R_{select}AKAP18 amino acids.

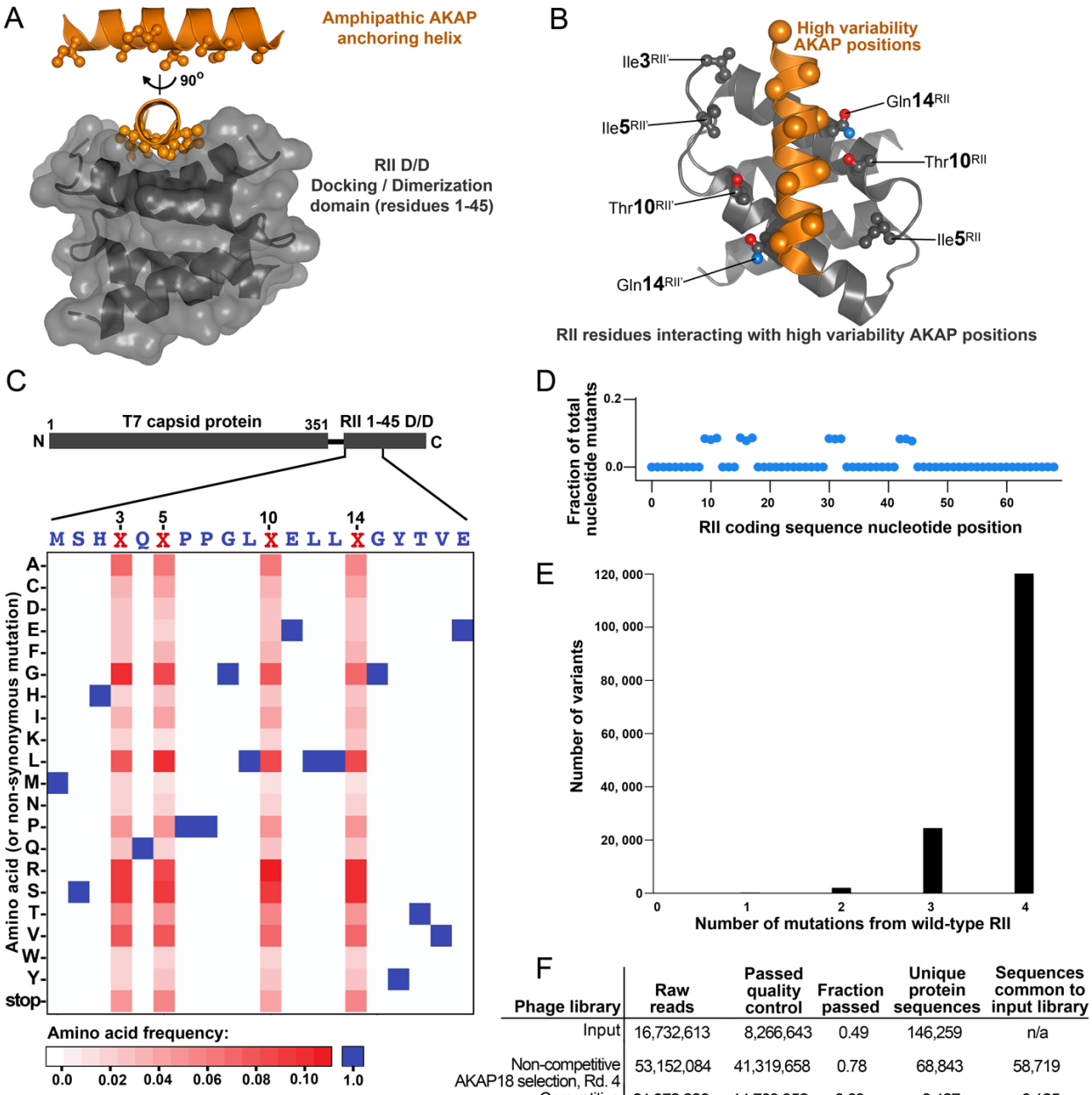

F

Phage library	Raw reads	Passed quality control	Fraction passed	Unique protein sequences	Sequences common to input library
Input	16,732,613	8,266,643	0.49	146,259	n/a
Non-competitive AKAP18 selection, Rd. 4	53,152,084	41,319,658	0.78	68,843	58,719
Competitive AKAP18 selection, Rd. 3	21,372,226	14,709,952	0.69	8,427	6,125

Figure 1

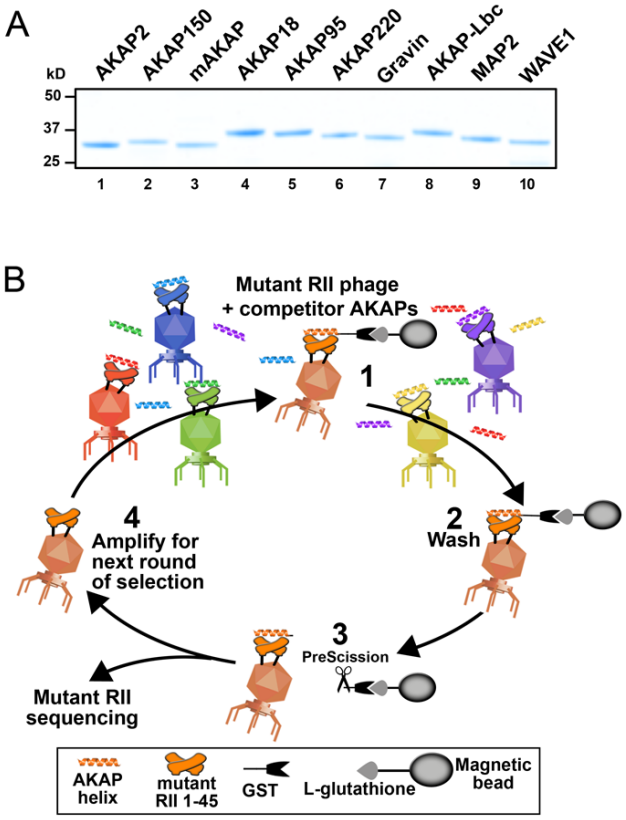

C

Native RII sequence: MSHIQIPPGLTELLQGYTVE

AKAP bait	Selection pressure	Sequence of selected mutant RII (1-20)
● AKAP2	High	MSHSQAPPGLRELLRGYTVE
● AKAP150	High	MSHLQRPPGLGELLQGYTVE
● AKAP18	High	MSHVQLPPGLDELLGGYTVE
AKAP-Lbc	High	MSHQQDPPGLGELLQGYTVE
AKAP220	High	MSHRQIPPGLFELLSGYTVE
mAKAP	Medium	MSHHQRPPGLKELLSGYTVE
Gravin	Medium	MSHGQAPPGLRELLGGYTVE
MAP2	Medium	MSHKQSPPGLGELLRGYTVE
AKAP95	None	MSHRQVPPGLRELLLGYTVE
WAVE1	None	MSHAQIPPGLEELLIGYTVE

Figure 2

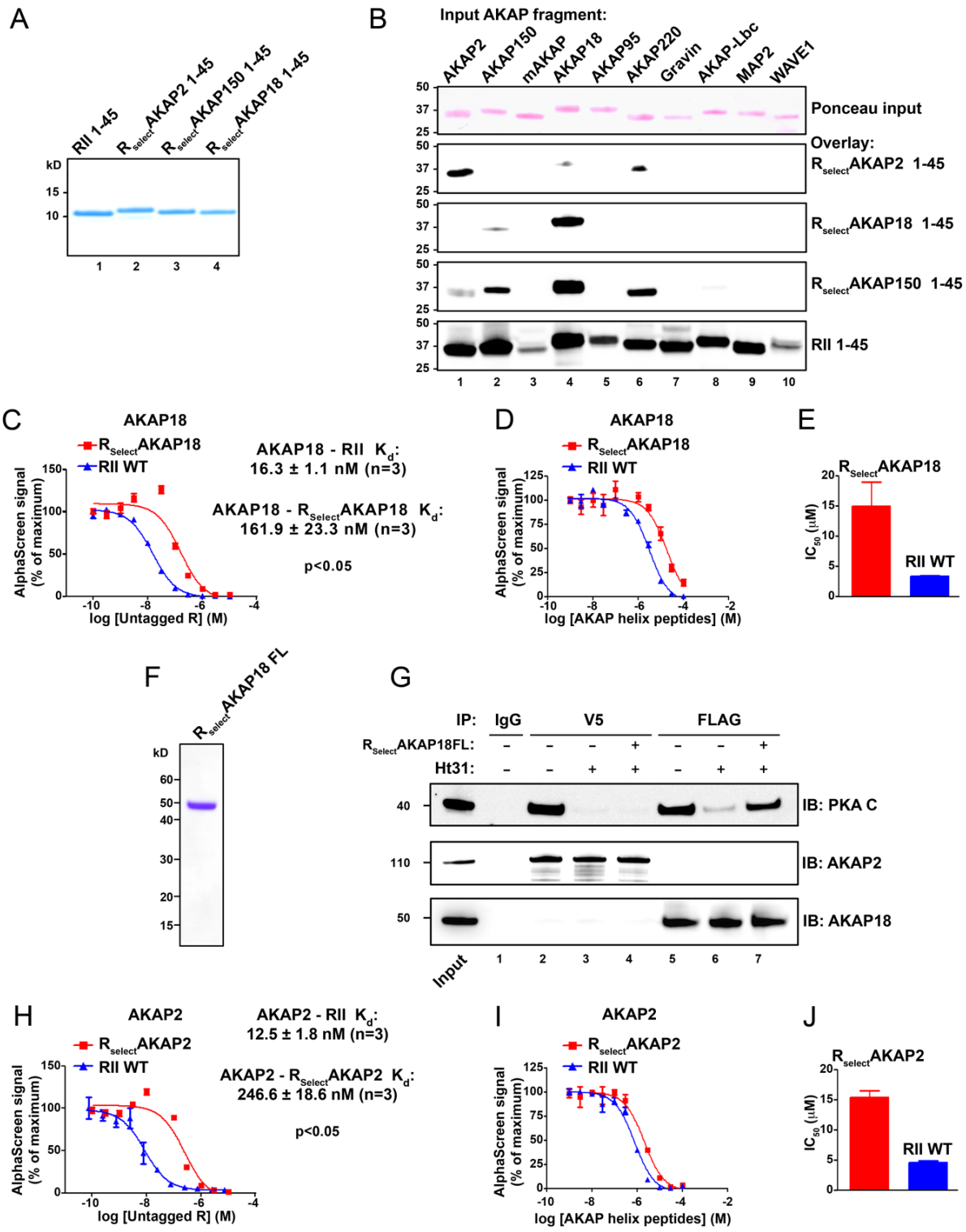

Figure 3

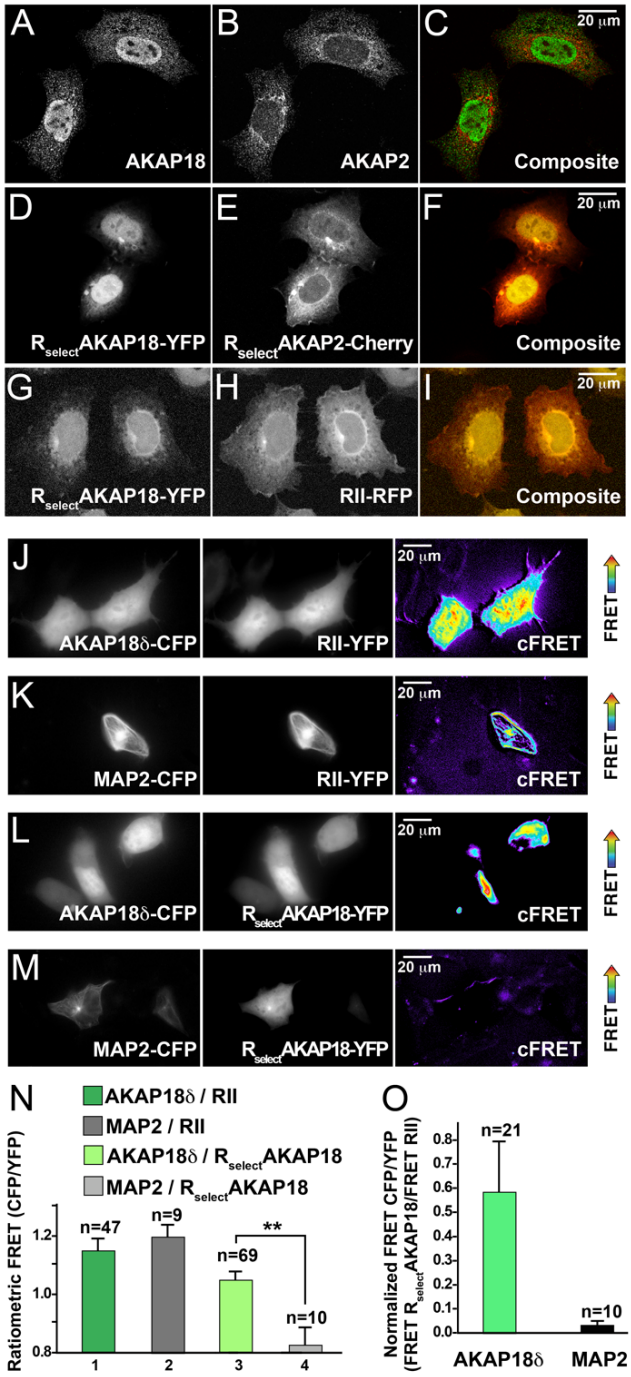

Figure 4

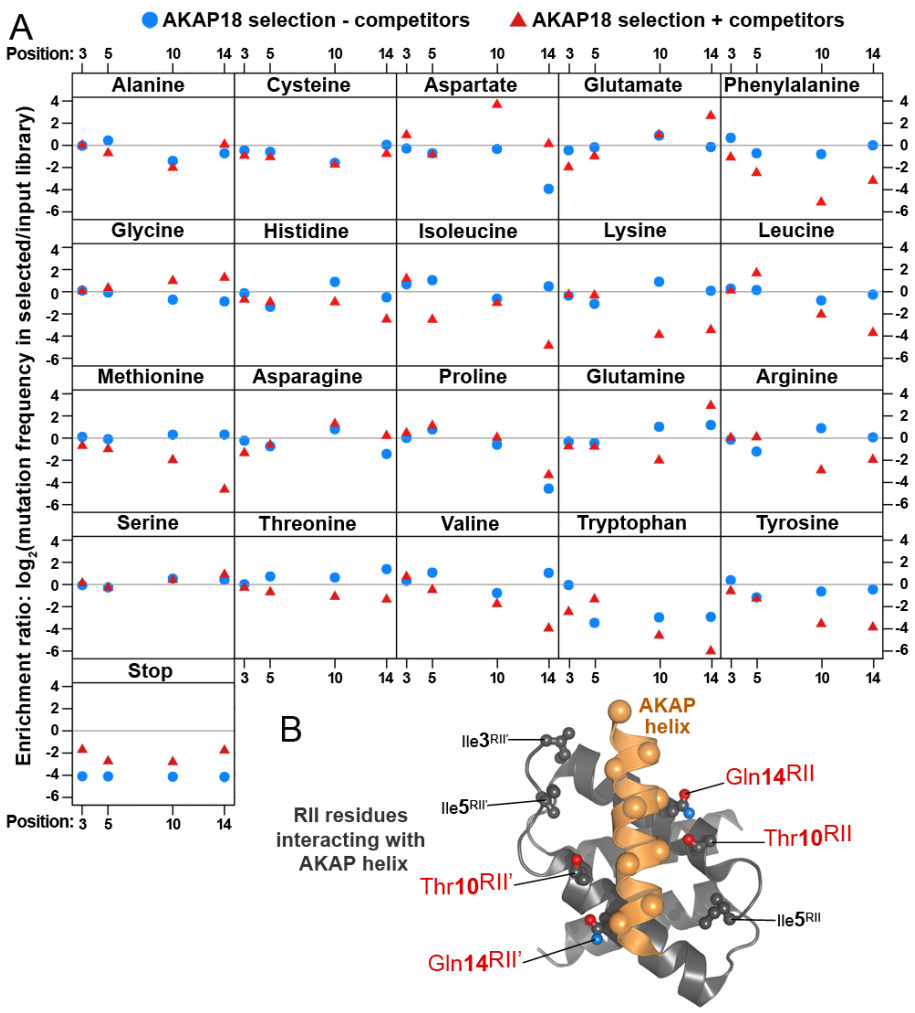

Figure 5

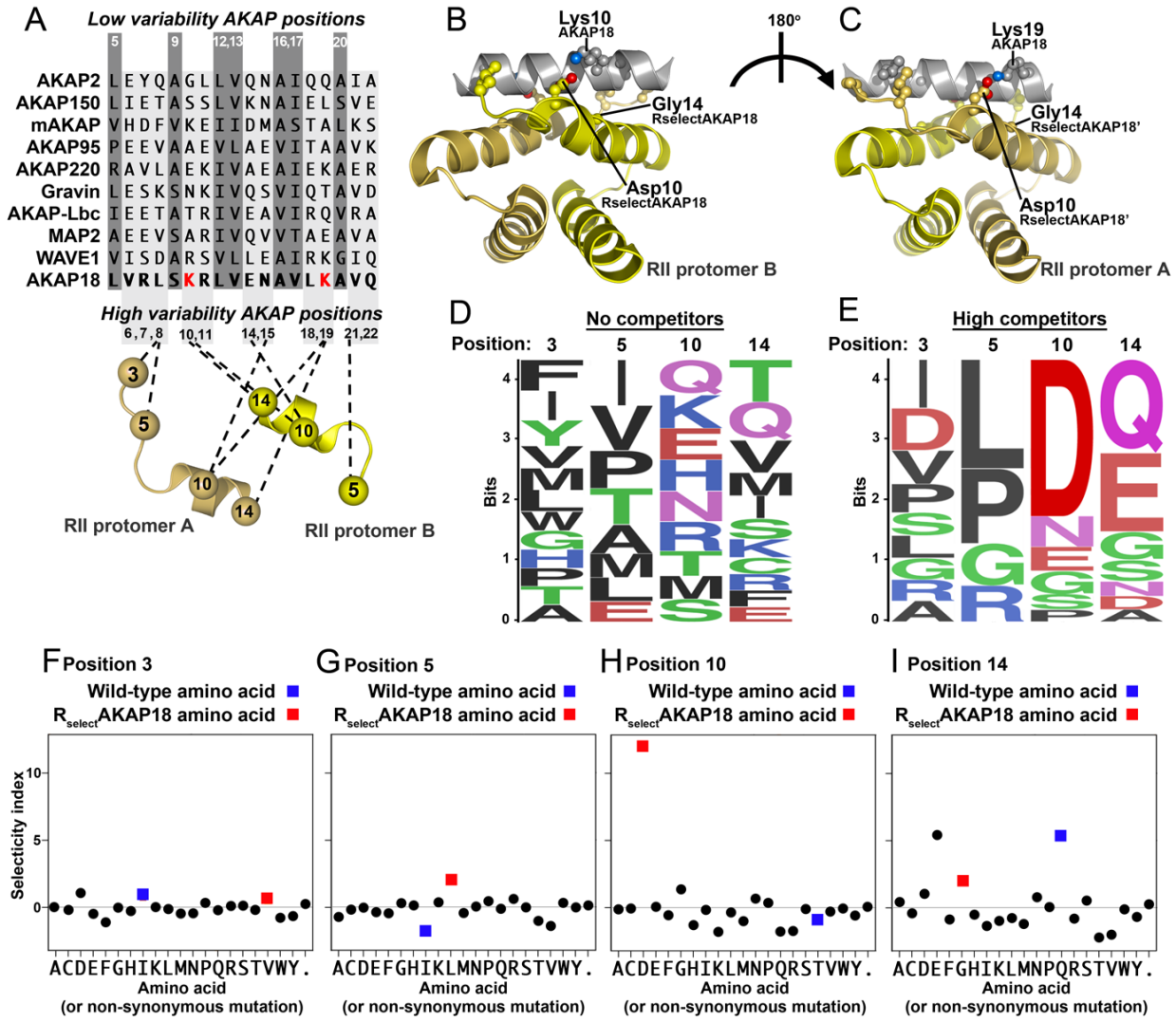

Figure 6